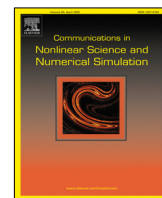




Contents lists available at ScienceDirect

# Communications in Nonlinear Science and Numerical Simulation

journal homepage: [www.elsevier.com/locate/cnsns](http://www.elsevier.com/locate/cnsns)



Research paper

## Identification of single- and double-well coherence-incoherence patterns by the binary distance matrix



Vagner dos Santos <sup>a,b</sup>, Matheus Rolim Sales <sup>c,d,e</sup>, Sishu Shankar Muni <sup>f</sup>,  
José Danilo Szezech Jr. <sup>a,c,\*</sup>, Antonio Marcos Batista <sup>a,c</sup>, Serhiy Yanchuk <sup>d,e</sup>,  
Jürgen Kurths <sup>d,g,h</sup>

<sup>a</sup> Department of Mathematics and Statistics, State University of Ponta Grossa, 84030-900, Ponta Grossa, PR, Brazil

<sup>b</sup> Ciências Exatas, Naturais e Engenharias, Centro Universitário UNIFATEB, 84266-010, Telêmaco Borba, PR, Brazil

<sup>c</sup> Graduate Program in Sciences/Physics, State University of Ponta Grossa, 84030-900, Ponta Grossa, PR, Brazil

<sup>d</sup> Potsdam Institute for Climate Impact Research, Member of the Leibniz Association, P.O. Box 6012 03, D-14412 Potsdam, Germany

<sup>e</sup> Institute of Mathematics, Humboldt University Berlin, 12489 Berlin, Germany

<sup>f</sup> Department of Physical Sciences, Indian Institute of Science Education and Research Kolkata, Mohanpur, West Bengal, 741246, India

<sup>g</sup> Institute of Physics, Humboldt University Berlin, 10099 Berlin, Germany

<sup>h</sup> Division of Dynamics, Lodz University of Technology, Stefanowskiego 1/15, 90-924 Lodz, Poland

### ARTICLE INFO

#### Article history:

Received 27 December 2022

Received in revised form 30 April 2023

Accepted 20 June 2023

Available online 25 June 2023

#### Keywords:

Chua circuit

Basin of attraction

Ring-star network

Coherence-incoherence

Single- and double-well dynamics

### ABSTRACT

The study of chimera states or, more generally, coherence-incoherence patterns has led to the development of several tools for their identification and characterization. In this work, we extend the eigenvalue decomposition method to distinguish between single-well (SW) and double-well (DW) patterns. By applying our method, we are able to identify the following four types of dynamical patterns in a ring of nonlocally coupled Chua circuits and nonlocally coupled cubic maps: SW cluster, SW coherence-incoherence pattern, DW cluster, and DW coherence-incoherence. In a ring-star network of Chua circuits, we investigate the influence of adding a central node on the spatio-temporal patterns. Our results show that increasing the coupling with the central node favors the occurrence of SW coherence-incoherence states. We observe that the boundaries of the attraction basins resemble fractal and riddled structures.

© 2023 Elsevier B.V. All rights reserved.

## 1. Introduction

Since Huygen's discovery of synchronization [1], coupled oscillators have became an important paradigm in nonlinear science. Numerous studies were devoted to synchronized and desynchronized oscillations. Kuramoto and Battogtokh [2] observed a coexistence of synchronous and asynchronous oscillations [3], known as chimera state [4], in a network of coupled phase oscillators. Since then chimera states have been studied in various systems ranging from chemical [5–8], electronic oscillators [9–11] to neuron systems [12–15]. Different classification schemes to identify chimera states were proposed [16,17]. Researchers have considered various topologies of networks to study the emergence of chimeras, such as ring-star [18], lattice [19–21], multiplex networks of both discrete [22,23] and continuous dynamical systems [24–26]. The effects of different coupling topologies have been investigated [17,27]. One motivation for such an exploration of

\* Corresponding author at: Department of Mathematics and Statistics, State University of Ponta Grossa, 84030-900, Ponta Grossa, PR, Brazil.  
E-mail addresses: [vagsantos@gmail.com](mailto:vagsantos@gmail.com) (V. dos Santos), [jdsjunior@uepg.br](mailto:jdsjunior@uepg.br) (J.D. Szezech Jr.).

topologies is that some neuronal dysfunctions might be associated with chimera states in the presence of certain network structures [28]. Chimera states were found in natural systems such as interacting fireflies or mechanical experiments [29].

Throughout the years, several measures have been used to identify and characterize these states, some examples are local and global order parameter [2,4,30,31], strength of incoherence [32], recurrence quantification analysis [33], spatial and temporal correlation measures [34], spatial inverse participation ratio [35] and eigenvalue decomposition [36]. Although they might be efficient in distinguishing between coherent, incoherent and chimera states, as far as our knowledge goes these measures are not able to separate states like single-well from double-well states. Meanwhile, many different patterns containing coherent and incoherent parts are often referred to as chimeras in the literature. Sometimes these patterns have no obvious relation to the chimera states originally described in [2], as in the case of our work. To avoid confusion, we use the more general term *coherence–incoherence patterns* in this work.

Multistability is a phenomenon that appears in a large class of dynamical systems. It refers to the coexistence of multiple attractors (at least two) in the dynamical system for the same set of parameter values. Different initial conditions in the phase space then leads to different attractors. From a dynamical perspective, the presence of multiple attractors is a striking feature. There are many studies in the literature with applications of multistability in neuroscience [37], optics [38], or engineering systems [39]. In an extreme case, infinitely many attractors can coexist [40]. Recently, a detailed geometric mechanism behind such a phenomenon was studied in Refs. [41,42]. The coexistence of two different coherence–incoherence states for the same set of parameter values was also observed. In a network of Chua's circuits [18,43] and in a network of cubic maps [43], it was verified that both single-well (SW) and double-well (DW) coherence–incoherence states coexist for the same parameter set. In that case, different initial conditions can induce different states, such as SW and DW coherence–incoherence states [18,43,44].

The Chua's circuit is known for its simplicity in terms of its components. It contains one inductor, one diode, two capacitors, and one nonlinear resistor [45]. The Chua's circuit has been applied in secure communication systems [46], Gaussian colored noise [47], and hand-written patterns recognition [48]. It is also well known for its double-scroll attractor. Different spatiotemporal patterns, for instance, spiral waves, have been found in networks of coupled Chua's oscillators [49]. As for the cubic map, it is the simplest map to present bistable dynamics and it can be thought as an analog of the Chua's circuit for discrete-time systems [50]. This map can demonstrate both regular and chaotic dynamics depending on its parameters, and the SW and DW coherence–incoherence states were observed in a network of coupled cubic maps with chaotic bistable dynamics [43].

The purpose of this work is threefold. (i) The first is to identify and characterize two different coherence–incoherence states, as well as cluster states, using an extension of the method of eigenvalue decomposition [36]. We use a network of Chua's circuits and a network of cubic maps to demonstrate our methodology. (ii) The second purpose is to explore the coexistence of spatio-temporal patterns, and the (iii) last one is to analyze the basins of attraction in the space of initial conditions. We study the coexistence of coherence–incoherence states in a network of Chua's circuits and compute the basins of attraction of each state present in the system for a set of parameters [51].

The paper is organized as follows. Section 2 illustrates the method used to characterize different network states such as cluster synchronization, desynchronization, SW coherence–incoherence state, and DW coherence–incoherence state. Section 3 introduces the ring-star network of Chua circuits and the network of cubic maps. Section 4 discusses the existence of bistability of coherence–incoherence states in the Chua's network and Section 5 presents our final remarks.

## 2. Methodology

Aiming to characterize the distinct dynamical states in a network of coupled oscillators, we extend the method of eigenvalue decomposition [36]. We begin by numerically integrating the equations of motion, in case of a flow, or by iterating the difference equations, in case of a mapping, to obtain the state variables time series  $\mathbf{x}_i(t)$ . We then construct the symmetric spatial distance matrix  $\mathbf{d}$ , according to

$$d_{ij} = \langle \|x_i(t) - x_j(t)\| \rangle_t, \quad (1)$$

where  $\|\cdot\|$  is the Euclidean norm,  $\langle \cdot \rangle_t$  denotes the average in time,  $i, j = 1, 2, \dots, N$ , and  $N$  is the network size. If  $d_{ij} \approx 0$ , the nodes  $i$  and  $j$  are coherent and large values of  $d_{ij}$  indicate incoherence. From  $\mathbf{d}$ , we define a binary matrix with elements equal to 1 and 0 denoting coherence and incoherence, respectively. These elements are computed as

$$L_{ij}^s = \Theta(\delta_s - d_{ij}), \quad (2)$$

where  $\delta_s > 0$  is a small threshold and  $\Theta$  is the Heaviside function. Defined this way,  $L_{ij}^s$  equals 1 if the absolute difference of  $x_i$  and  $x_j$  is smaller than  $\delta_s$  and zero otherwise. This definition of  $L_{ij}^s$  is similar to the definition of the recurrence matrix used in the recurrence quantification analysis [52–57], however, the recurrence matrix is evaluated using the time series of the state variables and our matrix is evaluated using the state variables of the nodes in the network. Such definition is often called spatial recurrence plot [33,58].

In the case of a completely incoherent state, the matrix  $\mathbf{L}^s$  is the identity matrix and all its eigenvalues are equal to 1. When some of the nodes are coherent, some off-diagonal elements of  $\mathbf{L}^s$  are nonzero and there are eigenvalues greater

than 1 and eigenvalues less than 1 in order to satisfy  $\sum_k \lambda_k = \text{tr}(\mathbf{L}^s) = N$ ,<sup>1</sup> where  $\text{tr}(\mathbf{L}^s)$  is the trace of  $\mathbf{L}^s$ . Parastesh et al. [36] reported that these eigenvalues are related to the coherent nodes and the corresponding eigenvectors show the positions of the synchronized nodes in the network. By comparing the elements of the eigenvectors, one can obtain the number of incoherent nodes of the network.

The drawback of this methodology is that one cannot apply it to large networks because the computational cost of the evaluation of eigenvalues and eigenvectors of large matrices is too high. One can, however, use the properties of the eigenvalues and eigenvectors reported by Parastesh et al. to simplify the method while getting the same results. Here we focus on the sum of the elements of each column of the binary matrix,  $s_j = \sum_i L_{ij}^s$ . If the  $j$ th node is incoherent with the rest of the network, then  $s_j = 1$ , as all elements of this column are zero except for the diagonal element. If there is coherence with another node, then  $s_j > 1$ . In this way, one can detect the positions of the synchronized nodes in the network.

### 3. Network models and pattern detection

In this study, we investigate the dynamics of a network of  $N + 1$  identical Chua's oscillators coupled in the ring-star topology and the dynamics of  $N$  identical cubic maps coupled in the ring topology. First we focus on finding how to distinguish between the different dynamical behaviors present in the systems using our methodology. Then, we study how spatio-temporal patterns change as a coupling parameter is varied.

#### 3.1. Chua circuits

The network topology of the coupled Chua's circuits is a mixture of the nonlocal circular ring topology, composed of  $N$  nodes, and the star topology. The dynamics of the nodes in the ring is given by

$$\begin{aligned}\dot{x}_i &= f_x(x_i, y_i, z_i) + k(x_{N+1} - x_i) + \frac{\sigma}{2rN} \sum_{j=i-rN}^{i+rN} (x_j - x_i), \\ \dot{y}_i &= f_y(x_i, y_i, z_i) + \frac{\sigma}{2rN} \sum_{j=i-rN}^{i+rN} (y_j - y_i), \\ \dot{z}_i &= f_z(x_i, y_i, z_i).\end{aligned}\tag{3}$$

for  $i = 1, 2, \dots, N$  and the indices are considered modulo  $N$ . The dynamics of the central node is given by

$$\begin{aligned}\dot{x}_{N+1} &= f_x(x_{N+1}, y_{N+1}, z_{N+1}) + \frac{k}{N} \sum_{j=1}^N (x_j - x_{N+1}), \\ \dot{y}_{N+1} &= f_y(x_{N+1}, y_{N+1}, z_{N+1}), \\ \dot{z}_{N+1} &= f_z(x_{N+1}, y_{N+1}, z_{N+1}).\end{aligned}\tag{4}$$

In Eqs. (3) and (4),  $x_i$ ,  $y_i$ , and  $z_i$  are the dynamical variables of the  $i$ th node,  $k \geq 0$  is the star topology coupling intensity, and  $\sigma \in [0, 1]$  and  $r \in [0, 0.5]$  are the coupling intensity and the coupling radius of the ring topology, respectively. The functions  $f_x$ ,  $f_y$ , and  $f_z$  are the governing equations of the uncoupled node, which have the following form for the Chua's circuit:

$$f_x = \alpha \left\{ y - x - \left[ Bx + \frac{1}{2}(A - B)(|x + 1| - |x - 1|) \right] \right\},\tag{5}$$

$$f_y = x - y + z,\tag{6}$$

$$f_z = -\beta y,\tag{7}$$

with the parameters  $A = -1.143$ ,  $B = -0.714$ ,  $\alpha = 9.4$ , and  $\beta = 14.28$ . For these parameter values, the Chua's system shows its well-known double-scroll regime [59]. The size of the ring network is set to  $N = 150$ , the coupling range to  $r = 1/3$ , the ring coupling strength to  $\sigma = 0.68$ , and the star coupling intensity to  $k = 0.005$ .

We consider parameters in which the oscillators stay in a single scroll attractor. These dynamic states have recently been called SW or DW [18]. In the case of a SW dynamics, all the oscillators in the network belong to the same region of the phase space. In the DW, the dynamics of a fraction of oscillators is constrained to a region of the phase space, whereas the rest of them are constrained to a different, symmetric region. We remark that the uncoupled as well as coupled system (3)–(4) of Chua's circuits possesses a central symmetry, i.e., the system is equivariant with respect to the transformation  $x_i \mapsto -x_i$ ,  $y_i \mapsto -y_i$ , and  $z_i \mapsto -z_i$  for all  $i$ . In particular, this guarantees a coexistence of two stable symmetric SW attractors in the uncoupled system.

<sup>1</sup> The binary distance matrix has the properties of the correlation matrix.

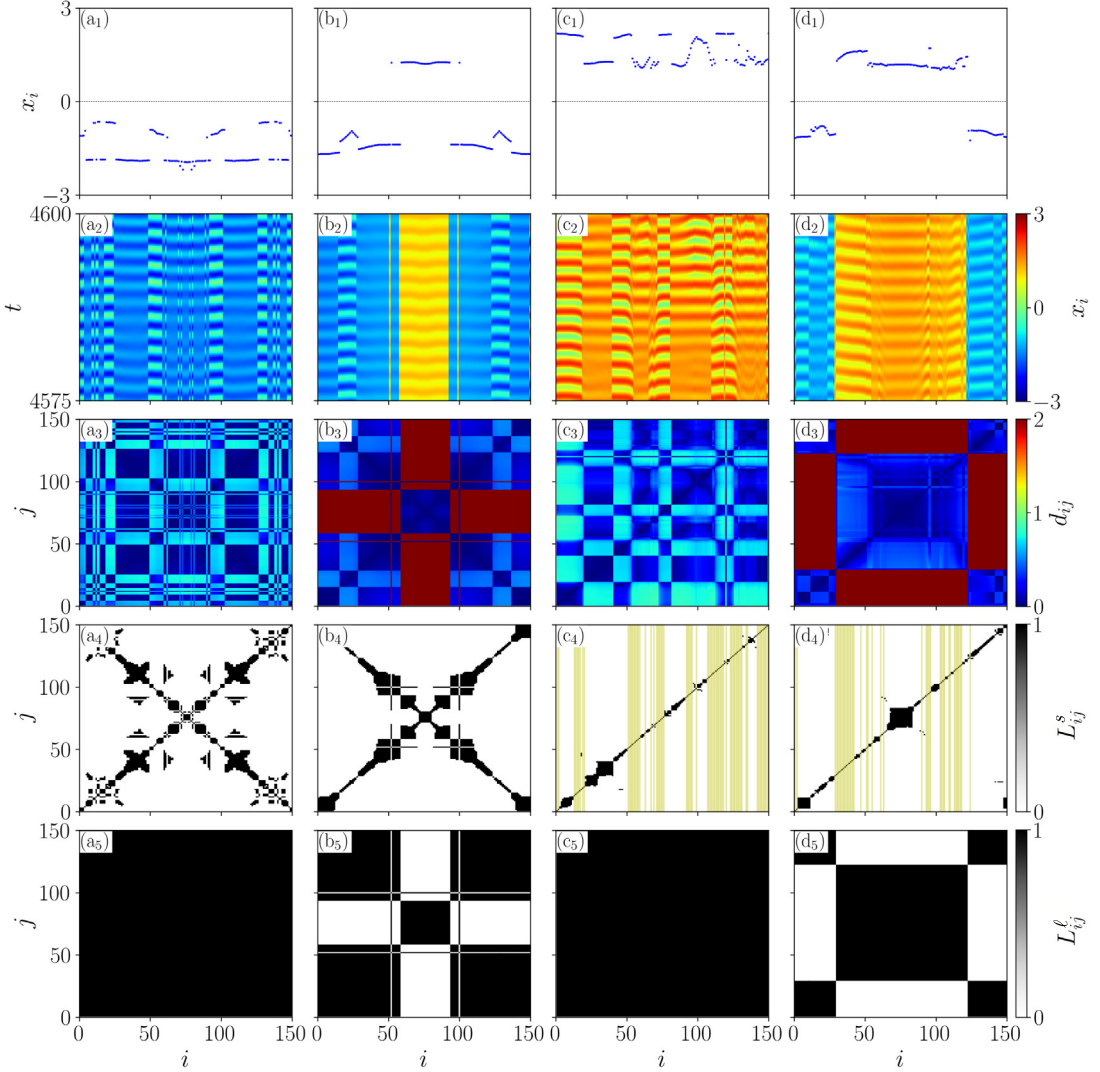


**Fig. 1.** The snapshots of  $x_i(t)$  at  $t = 4600$  (1st row) and the spatio-temporal evolution of  $x_i(t)$  (2nd row) of Eqs. (3) and (4), the distance matrix (3rd row), the binary distance matrix with a small threshold  $\delta_s$  with yellow vertical lines indicating the positions of the desynchronized nodes (4th row), and the binary distance matrix with a large threshold  $\delta_\ell$  (5th row) for (a) SW cluster state, (b) DW cluster state, (c) SW coherence-incoherence state, and (d) DW coherence-incoherence state. Parameters used are  $N = 150$ ,  $\sigma = 0.68$ ,  $r = 1/3$ ,  $k = 0.005$ ,  $\delta_s = 0.03$ ,  $\delta_\ell = 2.0$ ,  $A = -1.143$ ,  $B = -0.714$ ,  $\alpha = 9.4$ , and  $\beta = 14.28$ .

In order to observe these different dynamics, we consider all nodes to be at the unstable fixed point at the origin except for node  $i = 1$ , i.e.,  $(x_i, y_i, z_i) = (0, 0, 0)$  for  $i = 2, 3, \dots, N + 1$ . The first row of Fig. 1 shows the snapshots of  $x_i$  at  $t = 4600$  and the second row shows spatio-temporal evolution of  $x_i(t)$  for four different initial conditions, i.e., four different values of  $(x_1, y_1, z_1)$ . In Fig. 1(a<sub>1</sub>) we observe a SW cluster synchronization (SW-CL) dynamics [60–62]. In this case, the dynamics can be divided into two groups of oscillators with correlated dynamics, however the dynamics of all of them are roughly bound to the region  $x_i < 0$ . In Fig. 1(b<sub>1</sub>) we also observe the presence of groups of oscillators with correlated dynamics. In this second case, the dynamics of some of the oscillators are constrained to a region given roughly by  $x_i > 0$ , which is referred to as DW cluster synchronization (DW-CL). Fig. 1(c<sub>1</sub>) displays a SW dynamics, in which some oscillators are not coherent with any of the others. This state is referred to as SW coherence-incoherence state (SW-CI). Fig. 1(d<sub>1</sub>) exhibits a DW dynamics, where some of the oscillators are incoherent with the rest of the oscillators in the network. This last case is referred to as DW coherence-incoherence state (DW-CI).

In order to quantify whether the state of the network is a coherence-incoherence or a cluster synchronization pattern we proceed in the following way:

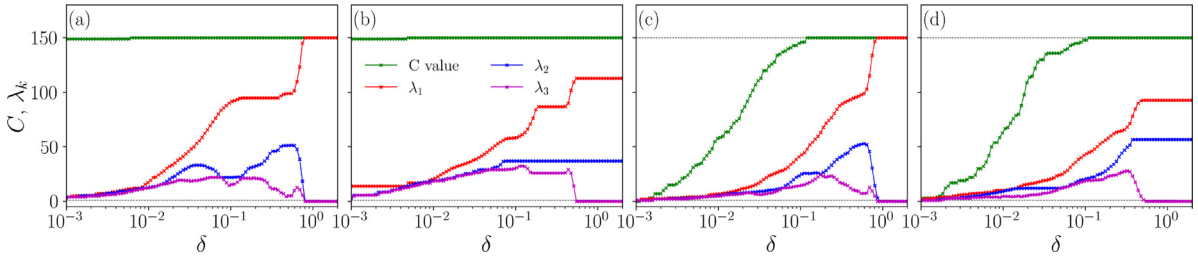


**Fig. 2.** The  $C$  value and the first three largest eigenvalues of the binary distance matrix as a function of the threshold  $\delta$  of the binary distance matrix of Chua's network. (a) SW cluster state, (b) DW cluster state, (c) SW coherence-incoherence state, and (d) DW coherence-incoherence state. Parameters used are  $N = 150$ ,  $\sigma = 0.68$ ,  $r = 1/3$ ,  $k = 0.005$ ,  $A = -1.143$ ,  $B = -0.714$ ,  $\alpha = 9.4$ , and  $\beta = 14.28$ .

1. Sum the elements of each column of the binary matrix:  $s_j = \sum_i I_{ij}^\delta$ , for  $i, j = 1, 2, \dots, N$ , i.e., excluding the central node.
2. Apply the sign function on the sum of each column as  $S_i = \text{sign}(s_i - 1)$ . This function assigns the value 1 to the coherent nodes, as  $s_i > 1$ , and the value 0 for the incoherent ones. Note that an incoherent node will have  $s_i = 1$ , so that the only nonzero element is the diagonal of the matrix, which will result in  $S_i = 0$ .
3. Sum the elements of  $S$ :  $C = \sum_{i=1}^N S_i$ .  $C = N$  represents cluster synchronization and  $C = 0$  shows that all the nodes are desynchronized. The coherence-incoherence state is characterized by intermediate values of  $C$ ,  $0 < C < N$ , i.e.,  $C$  nodes belong to synchronized clusters and  $N - C$  nodes are desynchronized.

We apply the above methodology to the states shown in the first row of Fig. 1. The third row of Fig. 1 shows the distance matrix  $d_{ij}$  and the fourth row of Fig. 1 displays the binary matrix  $I_{ij}^\delta$  of the corresponding states for a small threshold  $\delta_s = 0.03$ . For the first two states (a) and (b), every node is coherent with at least one other node of the network and, hence,  $C = N$  and we observe a cluster synchronization [36]. For the remaining two states (c) and (d), it holds  $C < N$ , and we identify the incoherent nodes as the ones whose row/column of the binary matrix has all elements equal to zero but the diagonal one. We plot yellow stripes in the panels (c<sub>1</sub>) and (d<sub>1</sub>) to emphasize these nodes.

The performed procedure allows us to distinguish among cluster, coherence-incoherence, and desynchronized states. However, this method alone does not differentiate between SW and DW dynamics. In order to accomplish this, we first note from Fig. 1 that for the DW dynamics some of the elements of the distance matrix are large when compared to the SW case. Thus, by changing the threshold  $\delta$ , we are able to differentiate between the SW and DW states. Indeed, the last row of Fig. 1 shows the binary matrix  $L_{ij}^\ell$  for a large threshold  $\delta_\ell = 2.0$ . For the SW cases, we see that all elements of the binary matrix equal 1 whereas for the DW cases some of them are 0. In this way, we can simply check if  $L_{ij}^\ell = 0$  for some  $i, j$ , and in the affirmative case, the state is a DW state.

In the recurrence analysis, there are several approaches to calculate the threshold  $\delta$ . Here, we make use of two threshold values,  $\delta_s$  and  $\delta_\ell$ , whose definition is based on the relation between the  $C$  value and the three largest eigenvalues of the binary recurrence matrix with  $\delta$ . To corroborate this methodology, we evaluate the  $C$  value and the first three largest eigenvalues of the binary matrix (red, blue, and purple, respectively) as a function of the threshold  $\delta$  (Fig. 2). We verify that for small values of  $\delta$ , the  $C$  value is equal to  $N$  for the cluster states. However, it is less than  $N$  for the coherence-incoherence states. Increasing  $\delta$ , the binary matrix has only one eigenvalue larger than 0 in the SW cases, which equals the size of the matrix, and it has two in the DW cases. This fact confirms our previous statement that for SW dynamics  $L_{ij}^\ell = 1$  for all  $i, j$ , as such a matrix has  $N - 1$  zero eigenvalues and one equal to  $N$ . Therefore, in order to distinguish among cluster, coherence-incoherence, and desynchronized states, we use a small threshold  $\delta_s = 0.03$  and calculate  $C$ . Then, we check if the binary matrix for a large threshold  $\delta_\ell = 2.0$  has all its elements equal to 1. If so, the state is SW, and DW otherwise. Lastly, in Fig. 3, we show in blue a snapshot of  $x_i(t)$  of the nodes at  $t = 4600$ . We separate the snapshots between SW and DW dynamics. In red, we plot the components of the vector  $S_i$ , which is used to identify coherent and incoherent regions in the network. And we also plot the projection of the dynamics of some sample nodes in the  $(x, y)$  plane for each case.

### 3.2. Cubic maps

Another paradigmatic system that was reported to show SW and DW dynamics is a network of coupled cubic maps, described by the following equations [43]:

$$x_i(n+1) = f_i(n) + \frac{\sigma}{2rN} \sum_{j=i-rN}^{i+rN} [f_j(n) - f_i(n)], \quad (8)$$

$$f_i(x) = (\alpha x_i - x_i^3) \exp\left(-\frac{x_i^2}{\beta}\right),$$

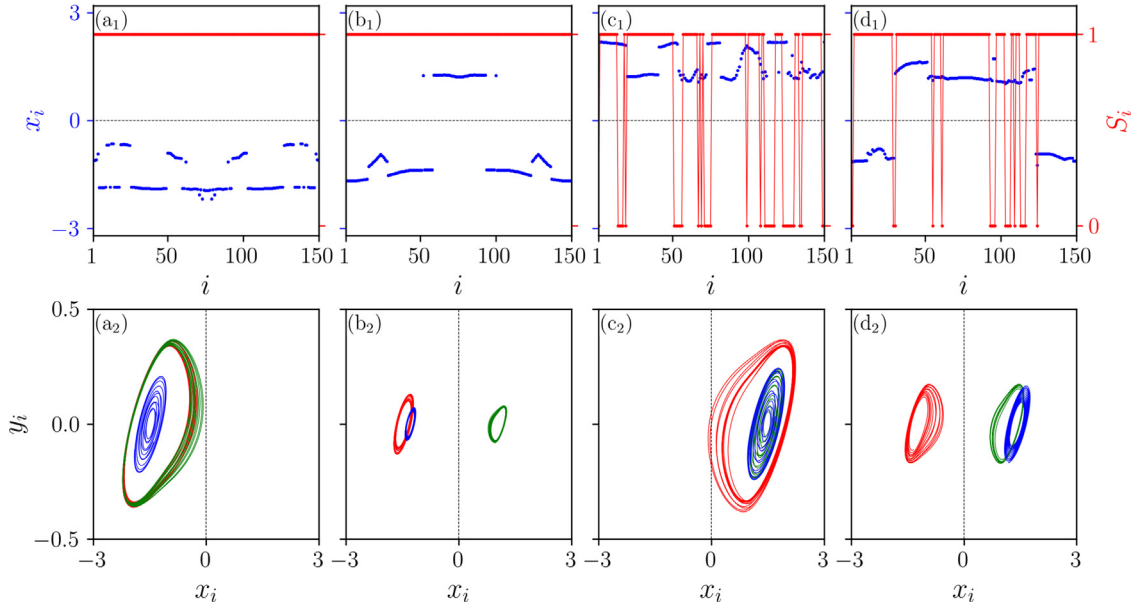


**Fig. 3.** (first row) Snapshots of  $x_i$  of the Chua's network at  $t = 4600$  and the vector  $S_i$ , and (second row) the phase space for three different nodes of a (a) SW cluster state, (b) DW cluster state, (c) SW coherence-incoherence state, and (d) DW coherence-incoherence state. Parameters used are  $N = 150$ ,  $\sigma = 0.68$ ,  $r = 1/3$ ,  $k = 0.005$ ,  $\delta_s = 0.03$ ,  $A = -1.143$ ,  $B = -0.714$ ,  $\alpha = 9.4$  and  $\beta = 14.28$ .

where  $i = 1, 2, \dots, N$ ,  $N$  is the size of the network,  $\sigma \in [0, 1]$  and  $r \in [0, 0.5]$  are the coupling strength and coupling radius, respectively, and  $\alpha$  and  $\beta$  are the control parameters of the map. The cubic map can be thought of as an analog of the Chua's circuit with chaotic dynamics for discrete-time systems and the cubic map is the simplest map to present bistable dynamics [50]. We remark here again the central symmetry  $x_i \mapsto -x_i$  leading to the emergence of symmetric coexisting attractors.

For the control parameters we set  $\alpha = 3$ ,  $\beta = 10$ , that correspond to a chaotic attractor of the map [43], and  $N = 300$  for the network size. As the coupling strength and coupling radius change, different regimes are observed in the system [43], such as complete chaotic synchronization, partial coherence with SW and DW structures, and SW and DW coherence-incoherence. By applying our methodology using the parameters  $(\sigma, r)$  reported in [43], we are indeed able to distinguish cluster synchronization from coherence-incoherence states and SW from DW as well. In Fig. 4 are shown the spatiotemporal evolution of  $x_i$  of the system (8) and in blue a snapshot of  $x_i$  at  $n = 1000$ , and in red we plot the components of the vector  $S_i$ . The parameters are (a)  $(\sigma, r) = (0.8, 0.275)$ , (b)  $(\sigma, r) = (0.6, 0.2)$ , (c) and (d)  $(\sigma, r) = (0.45, 0.2)$ , and we choose random initial conditions for all the nodes in the interval  $x \in [-2, 2]$ . For the coherence-incoherence detection, we use  $\delta_s = 0.06$  and for the SW/DW distinction  $\delta_\ell = 2.0$ .

For the first two states, Fig. 4(a) and (b), as all elements of  $S_i$  equal to 1, we get  $C = N$ , that corresponds to cluster synchronization. Whereas for the last two states, we observe  $C < N$ , indicating partial incoherence in the network. By increasing the threshold, as mentioned before, we are also able to distinguish between the SW states from the DW states.

Therefore, this methodology is a powerful tool in the detection of different dynamical behavior in networks of coupled oscillators. We would like to stress that the methodology proposed by Parastesh et al. [36] using the local order parameter matrix also gives similar results (not shown). However we use the distance matrix as it is simpler and it has a more direct interpretation in terms of synchronized/desynchronized states.

In the next section we employ our methodology to study how changes in the star coupling strength affects the spatial states of the network of  $N + 1$  Chua circuits, given by Eqs. (3) and (4).

#### 4. Coexistence of different states and parameter dependence

Here we study how spatio-temporal patterns change with varying parameters. Also, perturbed initial conditions can lead to completely different dynamics, due to complex structures of the basin of attraction [51,63]. As a first analysis of the influence of the central node on the ring network dynamics, we calculate the basin stability (BS) [64,65] for each of the four types of states in our network and its change when  $k$  is varied.

To estimate the value of BS, we consider 1000 random initial conditions in the interval  $[-1, 1]$  for  $x_1(0)$  and  $y_1(0)$ , and calculate the fraction of these points that converge to each of the four observable dynamics in the network. In that way, BS provides the proportion of the volumes of the basins of attraction for a given interval [66–68].

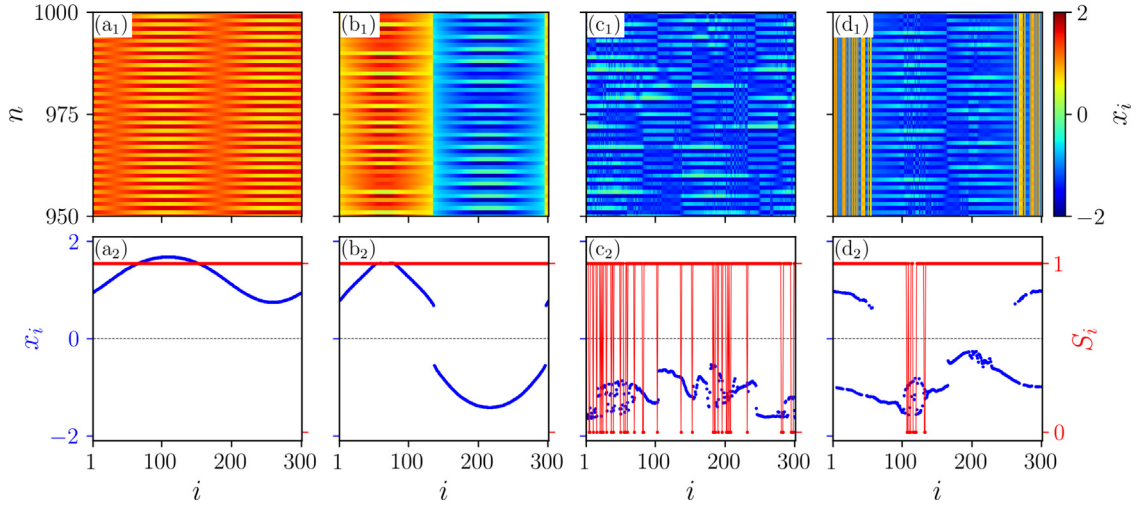


**Fig. 4.** The spatio-temporal evolution of  $x_i(n)$  of Eqs. (8) (first row), the snapshot of  $x_i$  at  $n = 1000$  in blue, and the components of the vector  $S_i$  in red (second row) for a (a) SW cluster with  $(\sigma, r) = (0.8, 0.275)$ , (b) DW cluster with  $(\sigma, r) = (0.6, 0.2)$ , (c) SW coherence-incoherence with  $(\sigma, r) = (0.45, 0.2)$  and (d) DW coherence-incoherence with  $(\sigma, r) = (0.45, 0.2)$ . The others parameters are  $\alpha = 3$ ,  $\beta = 10$ ,  $N = 300$ ,  $\delta_s = 0.06$  and  $\delta_\ell = 2.0$ .

In Fig. 5(a)–(c), we plot the value of BS obtained for  $k$  in the interval  $[0.0, 0.03]$  for three distinct network sizes (a)  $N = 125$ , (b)  $N = 150$ , and (c)  $N = 175$ . The color code used is as follows: blue for SW cluster states, green for DW cluster states, red for SW coherence-incoherence states, and yellow for DW coherence-incoherence states. From the graphs, we see that for  $k = 0$  the basins of all the states have approximately the same volume. By increasing the value of  $k$ , we verify that the basin of DW-CL begins to diminish so that from  $k = 0.015$ , those states are not observed in the network. We may also note that this happens independently of the network size  $N$ . By increasing  $k$  even further the basins of both SW-CL and DW-CI also get smaller, in a way that there is a dominance of SW-CI. The influence of the central node in the ring network dynamics is such that it privileges the SW-CI and suppresses the other types of dynamics observed for  $k = 0$ .

In Fig. 5(d)–(i) we plot the value of BS for the same range of  $k$ , but with fixed  $N = 150$  and varying the ring coupling parameter  $\sigma$ . This allows for an investigation about the parameter space  $(\sigma, k)$ . The coupling strengths used are (d)  $\sigma = 0.10$ , (e)  $\sigma = 0.25$ , (f)  $\sigma = 0.40$ , (g)  $\sigma = 0.68$ , (h)  $\sigma = 0.75$ , and (i)  $\sigma = 0.90$ . We can see from the graphs that an increase in the value of  $\sigma$  takes the distribution of states from mostly incoherent states, Fig. 5(d), to predominantly coherence-incoherence states of both single-well and double-well dynamics, Fig. 5(e)–(g), and then to the predominance of SW and DW cluster states, Fig. 5(h)–(i). We note that for these cases also, the increasing in  $k$  tends to increase the probability of observing SW dynamics, that being a consequence of the coupling with the central node.

In Fig. 6, we plot the basins of attraction for different values of  $k$ . To obtain the basins, we consider the initial conditions as  $(x_j, y_j, z_j) = (0, 0, 0)$  for  $j = 2, \dots, N + 1$  when  $t = 0$ , and vary  $x_1(0)$  and  $y_1(0)$  in the interval  $[-1, 1]$ . In other words, all nodes start at the unstable fixed point at the origin, except for node  $i = 1$ . For this node, the values of  $x_1(0)$  and  $y_1(0)$  are homogeneously distributed in the interval  $[-1, 1]$  using a grid of  $540 \times 540$ . Each initial condition is then numerically integrated and the dynamical state of the network after a total integration time  $t = 4600$  is analyzed. The color attributed to each point is blue for SW cluster states, green for DW cluster states, red for SW coherence-incoherence states, or yellow for DW coherence-incoherence states.

Without the presence of the central node (Fig. 6(a) and (b)), the basins show a very complex structure, with the basins of each of the states occupying a significant part of the given region. For  $k = 0.005$  (Fig. 6(c) and (d)), we perceive a very significant change in the structure of the basins, even though the change in BS is more subtle. Moreover, the magnifications of the regions indicated by the white rectangles (Fig. 6(b) and (d)) show that the boundaries of the basins resemble fractal and riddled structures [69,70]. In Fig. 6(e), we consider  $k = 0.0075$ , for this value the BS of DW-CL is larger (Fig. 5), and we find a significant decrease in the size of the basin of DW-CL. In Fig. 6(f), (g), and (h), we increase the central node coupling to  $k = 0.01$ ,  $k = 0.02$ , and  $k = 0.03$ , respectively. We see from these panels that the blue, green and yellow regions almost vanish, and mostly the basin of SW-CI remains, although riddled with points from the other basins.

To verify whether the basins in the  $x_1(0) \times y_1(0)$  space are indeed fractal, we measure the box-counting dimension through the uncertainty fraction method [71–73]. Given a region in this space, such as the ones depicted in Fig. 6, we consider a large number of randomly chosen initial conditions. For each initial condition, we check the final state of the network. We then perturb each initial condition in the  $x_1(0)$  direction by  $\pm\epsilon$ , and we check the final state of the network for these new two initial conditions. If either of the two perturbed initial conditions has a different result, we say the original initial condition is uncertain. The uncertainty fraction,  $f(\epsilon)$ , is the ratio between the number of uncertain initial conditions and the total number of them. We repeat these computations five times with 2000 initial conditions for each

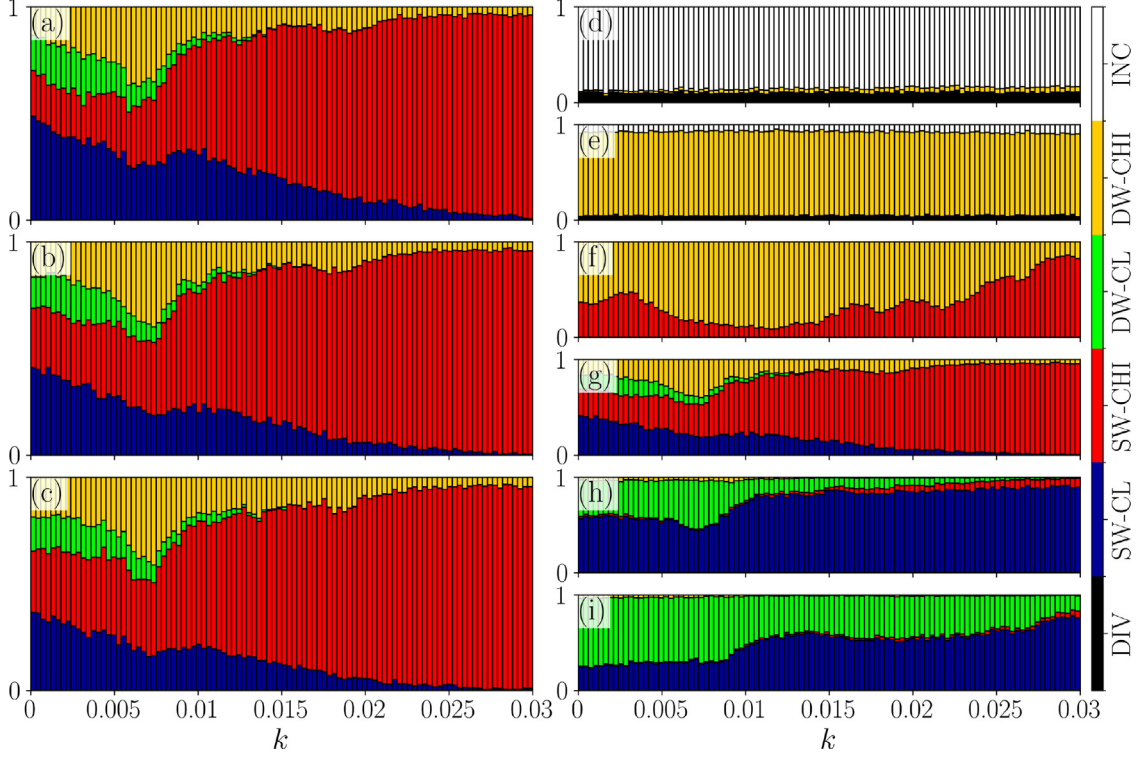


**Fig. 5.** Fraction of initial conditions that converges to each state as a function of  $k$  for Chua's network sizes (a)  $N = 125$ , (b)  $N = 150$ , and (c)  $N = 175$  with  $\sigma = 0.68$ , and for a fixed network size of  $N = 150$  with coupling strengths (d)  $\sigma = 0.10$ , (e)  $\sigma = 0.25$ , (f)  $\sigma = 0.40$ , (g)  $\sigma = 0.68$ , (h)  $\sigma = 0.75$ , and (i)  $\sigma = 0.90$ . The initial conditions were taken from a uniform random distribution in the interval  $[-1, 1]$  for  $x_1(0)$  and  $y_1(0)$  with  $z_1(0) = 0$ . The color code used is black for divergent states, blue for SW cluster states, green for DW cluster states, red for SW coherence-incoherence states, yellow for DW coherence-incoherence states, and white for incoherence states. Other parameters are  $r = 1/3$ ,  $\delta_s = 0.03$ ,  $\delta_\ell = 2.0$ ,  $A = -1.143$ ,  $B = -0.714$ ,  $\alpha = 9.4$ , and  $\beta = 14.28$ .

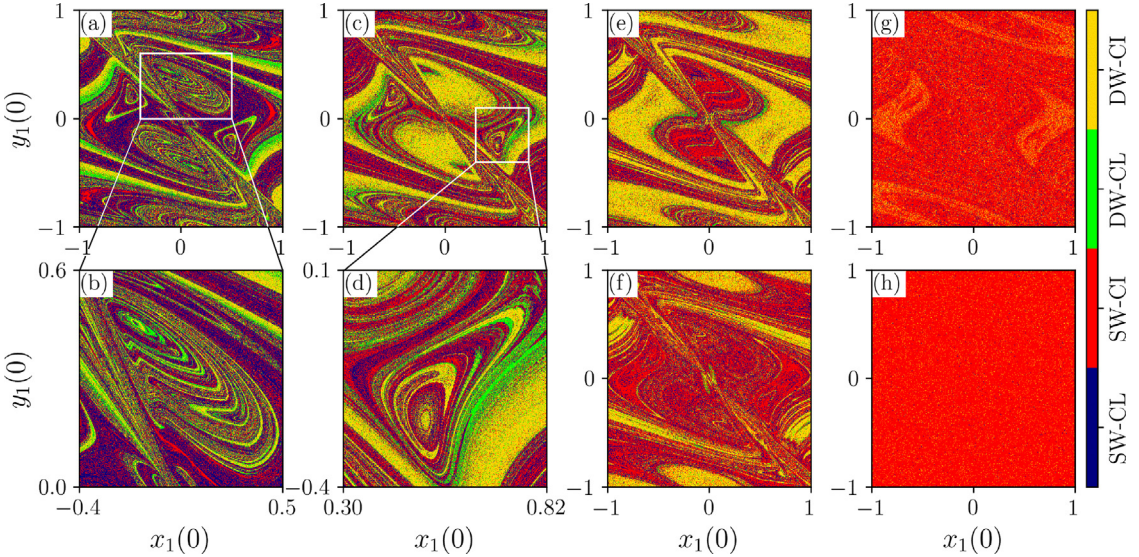


**Fig. 6.** Basins of attraction of the ring-star network of Chua's circuits in a grid of  $540 \times 540$  initial conditions for different  $k$  values. In (a) and (b)  $k = 0.0$ , (c) and (d)  $k = 0.005$ , (e)  $k = 0.0075$ , (f)  $k = 0.01$ , (g)  $k = 0.02$ , and (h)  $k = 0.03$ . The color code used is blue for SW cluster states, green for DW cluster states, red for SW coherence-incoherence states, and yellow for DW coherence-incoherence states. Other parameters are  $N = 150$ ,  $\sigma = 0.68$ ,  $r = 1/3$ ,  $\delta_s = 0.03$ ,  $\delta_\ell = 2.0$ ,  $A = -1.143$ ,  $B = -0.714$ ,  $\alpha = 9.4$ , and  $\beta = 14.28$ .

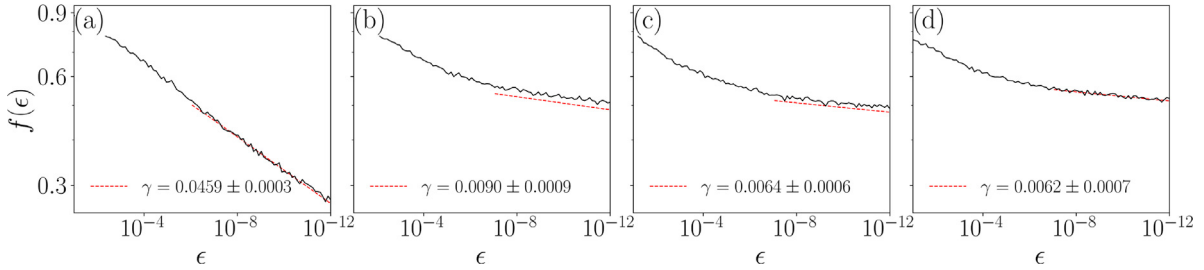


**Fig. 7.** The uncertainty fraction for (a)  $k = 0.0$ , (b)  $k = 0.005$ , (c)  $k = 0.0075$ , and (d)  $k = 0.01$ . The dashed red lines indicate the slope of  $f(\epsilon)$ . Each point is the average of four computations with 2000 distinct initial conditions. Other parameters are  $N = 150$ ,  $\sigma = 0.68$ ,  $r = 1/3$ ,  $\delta_s = 0.03$ ,  $\delta_\ell = 2.0$ ,  $A = -1.143$ ,  $B = -0.714$ ,  $\alpha = 9.4$ , and  $\beta = 14.28$ .

value of  $\epsilon$ , which we vary from  $10^{-1}$  to  $10^{-12}$ . For smooth basins,  $f(\epsilon) \sim \epsilon$ . If the basin is fractal,  $f(\epsilon)$  is expected to scale with  $\epsilon$  as

$$f(\epsilon) \sim \epsilon^\gamma, \quad (9)$$

where  $\gamma$  is the uncertainty exponent. We compute the uncertainty exponent for each one of the five computations and take its mean and standard deviation:  $\gamma = \bar{\gamma} \pm \sigma_\gamma$ .

It is possible to express the box-counting dimension in terms of the uncertainty exponent. Let  $D$  be the dimension of the space and  $N(\eta)$  be the minimum number of  $D$ -dimensional boxes of length  $\eta$  necessary to cover the basin's boundary. The box-counting dimension of the latter is

$$d = \lim_{\eta \rightarrow 0} \frac{\ln N(\eta)}{\ln 1/\eta}, \quad (10)$$

such that  $N(\eta) \sim \eta^{-d}$  for  $\eta$  small enough. By setting  $\eta \equiv \epsilon$ , the volume of the uncertain region is  $N(\epsilon)\epsilon^D \sim \epsilon^{D-d}$ , where  $\epsilon^D$  is the volume of the boxes. Therefore, the uncertainty exponent is [72]

$$\gamma = D - d. \quad (11)$$

In our case,  $D = 2$  and a smooth boundary, which has  $d = 1$ , has  $\gamma = 1$ , whereas a fractal boundary is characterized by  $\gamma \in (0, 1)$ . Fractal structures can be found in a variety of nonlinear systems [74]. The presence of fractal boundaries in these systems obstructs predictability [71], and  $f(\epsilon)$  can be understood as a measure of this unpredictability. In cases where the boundaries are fractal, a significant reduction in the initial condition uncertainty  $\epsilon$  may be necessary to minimize the uncertainty in the final state.

The uncertainty exponent can be estimated from the slope in the  $\log f(\epsilon)$ - $\log \epsilon$  plot (Fig. 7). For  $k = 0.0$ , we obtain an uncertainty exponent of  $\gamma = 0.0459 \pm 0.0003$ , and a dimension of  $d = 1.9541 \pm 0.0003$ , which means the basin indeed exhibits fractal structures. The uncertainty exponents for  $k = 0.005$ ,  $0.0075$ , and  $0.01$  are very small, and the dimensions are approximately equal to  $D = 2$ . This is an indication of the existence of a riddled basin: the probability of finding an uncertain initial condition,  $f(\epsilon)$ , is constant regardless of the size of the initial condition uncertainty,  $\epsilon$ . In other words, decreasing the uncertainty in the initial condition does not decrease the uncertainty in the final state.

## 5. Conclusions

We have analyzed the influence of a central node in a network of nonlocally coupled systems. We first characterized the dynamical states in a network of Chua's oscillators and in a network of cubic maps. By considering two values of the threshold to define the binary matrix  $\mathbf{L}$ , we were able to separate the dynamics among SW cluster states, SW coherence-incoherence states, DW cluster states, and DW coherence-incoherence states. We have also tested whether the maximum distance, instead of the mean distance, in the definition (1), should be a better choice. However our simulations indicated that is not the case, as the maximum distance detected some false positive DW states (not shown).

The estimation of basin stability allowed us to verify how the probability of obtaining each state changes by increasing the strength of the central node coupling  $k$ . This analysis showed that the influence of the central node causes the suppression of some dynamical states, increasing the size of SW-CI basin. Although it allows us to see the fraction of initial conditions that converge to each state, BS alone cannot tell us much about the structures in the basins. From Fig. 6, we see that the structures are very complex and the magnifications (Fig. 6(b) and (d)) show that the basins may have fractal and riddled structures. This hypothesis is confirmed by the estimate of the uncertainty fraction for these basins (Fig. 7(a)-(d)). From these figures, we verify that the changes in the proportions of each state happens simultaneously with drastic changes in their boundaries. For larger values of  $k$ , the basin of SW-CI dominates and is riddled with points of the other states.

An interesting point for future studies could be a more detailed analysis of a coexistence of different coherence-incoherence patterns. Indeed, our method allows to distinguish four big classes of patterns: SW and DW clusters, SW and DW coherence-incoherence patterns. However, it is obvious that there can be a high multistability within each class of these solutions, which makes the problem even more challenging. Also, one limitation of our method is the necessity of stability of the coherence-incoherence pattern over some time interval. Patterns in which the position and size of the incoherent region are too unstable hinder the correct identification of such regions. The situation can become even more complicated if the dynamics of the node has a more complicated symmetry than a central symmetry considered in our work. For example,  $S^n$  symmetry may lead to a coexistence of  $n$  symmetric attractors in the node's dynamics which could lead to  $n$ -well states. In the same direction, the studies of these patterns in higher-order interaction networks could be another perspective for future research. Recently, the studies on this direction has been started [75,76] and the understanding is not yet completed.

## CRediT authorship contribution statement

**Vagner dos Santos:** Formal analysis, Investigation. **Matheus Rolim Sales:** Formal analysis, Investigation. **Sishu Shankar Muni:** Formal analysis, Investigation. **José Danilo Szezech Jr.:** Writing – review & editing. **Antonio Marcos Batista:** Writing – review & editing. **Serhiy Yanchuk:** Writing – review & editing. **Jürgen Kurths:** Writing – review & editing.

## Declaration of competing interest

The authors declare that they have no known competing financial interests or personal relationships that could have appeared to influence the work reported in this paper.

## Data availability

Data will be made available on request.

## Acknowledgments

We wish to acknowledge the support of the Araucária Foundation, the Coordination of Superior Level Staff Improvement (CAPES) and the National Council for Scientific and Technological Development (CNPq). S.S.M acknowledges the School of Fundamental Sciences doctoral bursary funding, Massey University during this research. S.S.M acknowledges the use of NeSI (New Zealand e-Science Infrastructure) HPC computing facilities during the elementary stages of this research. V. S acknowledges Fatemeh Parastesh for the help in understanding the chimera states detection using eigenvalue decomposition. S.Y. was supported by the German Research Foundation DFG, Project No. 411803875. J.K. has been supported by the Alexander von Humboldt Polish Honorary Research Scholarship 2020 of the Foundation for Polish Science. We would also like to thank the 105 Group Science ([www.105groupscience.com](http://www.105groupscience.com)) for fruitful discussions.

## References

- [1] Willms AR, Kitanov PM, Langford WF. Huygens' clocks revisited. *R Soc Open Sci* 2017;4(9):170777.
- [2] Kuramoto Y, Battogtokh D. Coexistence of coherence and incoherence in nonlocally coupled phase oscillators. *Nonlinear Phenom Complex Syst* 2002;5:380–5.
- [3] Montbrió E, Kurths J, Blasius B. Synchronization of two interacting populations of oscillators. *Phys Rev E* 2004;70:056125.
- [4] Abrams DM, Strogatz SH. Chimera states for coupled oscillators. *Phys Rev Lett* 2004;93:174102.
- [5] Tinsley MR, Nkomo S, Showalter K. Chimera and phase-cluster states in populations of coupled chemical oscillators. *Nat Phys* 2012;8(9):662–5.
- [6] Nkomo S, Tinsley MR, Showalter K. Chimera states in populations of nonlocally coupled chemical oscillators. *Phys Rev Lett* 2013;110:244102.
- [7] Totz JF, Rode J, Tinsley MR, Showalter K, Engel H. Spiral wave chimera states in large populations of coupled chemical oscillators. *Nat Phys* 2018;14(3):282–5.
- [8] Haugland SW, Tosolini A, Krischer K. Between synchrony and turbulence: intricate hierarchies of coexistence patterns. *Nature Commun* 2021;12(1):5634.
- [9] Rosin DP, Rontani D, Haynes ND, Schöll E, Gauthier DJ. Transient scaling and resurgence of chimera states in networks of Boolean phase oscillators. *Phys Rev E* 2014;90:030902.
- [10] Gambuzza LV, Buscarino A, Chessaari S, Fortuna L, Meucci R, Frasca M. Experimental investigation of chimera states with quiescent and synchronous domains in coupled electronic oscillators. *Phys Rev E* 2014;90:032905.
- [11] Hart JD, Bansal K, Murphy TE, Roy R. Experimental observation of chimera and cluster states in a minimal globally coupled network. *Chaos* 2016;26(9):094801.
- [12] Santos MS, Szezech JD, Borges FS, Iarosz KC, Caldas IL, Batista AM, Viana RL, Kurths J. Chimera-like states in a neuronal network model of the cat brain. *Chaos Solitons Fractals* 2017;101:86–91.
- [13] Majhi S, Perc M, Ghosh D. Chimera states in uncoupled neurons induced by a multilayer structure. *Sci Rep* 2016;6(1):1–11.
- [14] Majhi S, Perc M, Ghosh D. Chimera states in a multilayer network of coupled and uncoupled neurons. *Chaos* 2017;27(7):073109.
- [15] Majhi S, Bera BK, Ghosh D, Perc M. Chimera states in neuronal networks: A review. *Phys Life Rev* 2019;28:100–21.
- [16] Omel'chenko OE. The mathematics behind chimera states. *Nonlinearity* 2018;31(5):R121.
- [17] Schöll E. Synchronization patterns and chimera states in complex networks: Interplay of topology and dynamics. *Eur Phys J Spec Top* 2016;225(6):891–919.
- [18] Muni SS, Provata A. Chimera states in ring-star network of Chua circuits. *Nonlinear Dynam* 2020;101:2509–21.

- [19] Shepelev IA, Bukh AV, Muni SS, Anishchenko VS. Role of solitary states in forming spatiotemporal patterns in a 2D lattice of van der Pol oscillators. *Chaos Solitons Fractals* 2020;135:109725.
- [20] Shepelev IA, Bukh AV, Muni SS. Quantifying the transition from spiral waves to spiral wave chimeras in a lattice of self-sustained oscillators. *Regul Chaotic Dyn* 2020;25:597–615.
- [21] Omel'chenko OE, Wolfrum M, Yanchuk S, Maistrenko YL, Sudakov O. Stationary patterns of coherence and incoherence in two-dimensional arrays of non-locally-coupled phase oscillators. *Phys Rev E* 2012;85(3):036210.
- [22] Muni SS, Rajagopal K, Karthikeyan A, Arun S. Discrete hybrid Izhikevich neuron model: Nodal and network behaviours considering electromagnetic flux coupling. *Chaos Solitons Fractals* 2022;155:111759.
- [23] Muni SS, Fatoyinbo HO, Ghosh I. Dynamical effects of electromagnetic flux on Chialvo neuron map: nodal and network behaviors. *Int J Bifurcation Chaos* 2022;32(09):2230020.
- [24] Shepelev IA, Muni SS, Schöll E, Strelkova GI. Repulsive inter-layer coupling induces anti-phase synchronization. *Chaos* 2021;31(6):063116.
- [25] Shepelev IA, Muni SS, Vadivasova TE. Synchronization of wave structures in a heterogeneous multiplex network of 2D lattices with attractive and repulsive intra-layer coupling. *Chaos* 2021;31(2):021104.
- [26] Shepelev IA, Muni SS, Vadivasova TE. Spatiotemporal patterns in a 2D lattice with linear repulsive and nonlinear attractive coupling. *Chaos* 2021;31(4):043136.
- [27] Martens EA, Panaggio MJ, Abrams DM. Basins of attraction for chimera states. *New J Phys* 2016;18(2):022002.
- [28] Uhlhaas PJ, Singer W. Neural synchrony in brain disorders: Relevance for cognitive dysfunctions and pathophysiology. *Neuron* 2006;52(1):155–68.
- [29] Dudkowski D, Jaros P, Czolczyński K, Kapitaniak T. Small amplitude chimeras for coupled clocks. *Nonlinear Dynam* 2020;102(3):1541–52.
- [30] Omel'chenko OE, Maistrenko YL, Tass PA. Chimera states: The natural link between coherence and incoherence. *Phys Rev Lett* 2008;100:044105.
- [31] Batista CA, Viana RL. Quantifying coherence of chimera states in coupled chaotic systems. *Phys A* 2019;526:120869.
- [32] Gopal R, Chandrasekar VK, Venkatesan A, Lakshmanan M. Observation and characterization of chimera states in coupled dynamical systems with nonlocal coupling. *Phys Rev E* 2014;89:052914.
- [33] Santos MS, Szezech JD, Batista AM, Caldas IL, Viana RL, Lopes SR. Recurrence quantification analysis of chimera states. *Phys Lett A* 2015;379(37):2188–92.
- [34] Kemeth FP, Haugland SW, Schmidt L, Kevrekidis IG, Krischer K. A classification scheme for chimera states. *Chaos* 2016;26(9):094815.
- [35] Ghosh S, Jalan S. Engineering chimera patterns in networks using heterogeneous delays. *Chaos* 2018;28(7):071103.
- [36] Parastesh F, Azarnoush H, Jafari S, Perc M. Detecting chimeras by eigenvalue decomposition of the bivariate local order parameter. *EPL (Europhys Lett)* 2020;130(2):28003.
- [37] Malashchenko T, Shilnikov A, Cymbalyuk G. Six types of multistability in a Neuronal model based on slow calcium current. *PLoS ONE* 2011;6(7):1–10.
- [38] Yanchuk S, Wolfrum M. A multiple time scale approach to the stability of external cavity modes in the Lang–Kobayashi system using the limit of large delay. *SIAM J Appl Dyn Syst* 2010;9(2):519–35.
- [39] Feudel U, Pisarchik AN, Showalter K. Multistability and tipping: From mathematics and physics to climate and brain—Minireview and preface to the focus issue. *Chaos* 2018;28(3):033501.
- [40] Newhouse SE. Diffeomorphisms with infinitely many sinks. *Topology* 1974;13(1):9–18.
- [41] Muni SS. Globally resonant homoclinic tangencies. 2022.
- [42] Muni SS, McLachlan RJ, Simpson DJW. Homoclinic tangencies with infinitely many asymptotically stable single-round periodic solutions. *Discrete Contin Dyn Syst Ser A* 2021;41(8):3629–50.
- [43] Shepelev IA, Bukh AV, Strelkova GI, Vadivasova TE, Anishchenko VS. Chimera states in ensembles of bistable elements with regular and chaotic dynamics. *Nonlinear Dynam* 2017;90(4):2317–30.
- [44] Shepelev IA, Vadivasova TE, Bukh AV, Strelkova GI, Anishchenko VS. New type of chimera structures in a ring of bistable FitzHugh–Nagumo oscillators with nonlocal interaction. *Phys Lett A* 2017;381(16):1398–404.
- [45] Chua LO. The Genesis of Chua's circuit. *AEÜ Int J Electron Commun* 1992;46(4).
- [46] Lozi R. Secure communications via chaotic synchronization in Chua's circuit and Bonhoeffer–Van der Pol equation: numerical analysis of the errors of the recovered signal. In: Proceedings of ISCAS'95 – International symposium on circuits and systems, Vol. 1. 1995, p. 684–7.
- [47] Ando B, Baglio S, Graziani S, Pitrone N. CNNs for noise generation in dithered transducers. In: Proceedings of the 17th IEEE instrumentation and measurement technology conference [Cat. No. 00CH37066], Vol. 2. 2000, p. 1071–6.
- [48] Baird B, Hirsch MW, Eeckman F. A neural network associative memory for handwritten character recognition using multiple Chua characters. *IEEE Trans Circuits Syst II* 1993;40(10):667–74.
- [49] Perez-Munuzuri A, Perez-Munuzuri V, Perez-Villar V, Chua LO. Spiral waves on a 2-D array of nonlinear circuits. *IEEE Trans Circuits Syst I* 1993;40(11):872–7.
- [50] Skjolding H, Branner-Jørgensen B, Christiansen PL, Jensen HE. Bifurcations in discrete dynamical systems with cubic maps. *SIAM J Appl Math* 1983;43(3):520–34.
- [51] Santos V, Szezech JD, Batista AM, Iarosz KC, Baptista MS, Ren HP, Grebogi C, Viana RL, Caldas IL, Maistrenko YL, Kurths J. Riddling: Chimera's dilemma. *Chaos* 2018;28(8):081105.
- [52] Eckmann JP, Kamphorst SO, Ruelle D. Recurrence plots of dynamical systems. *Europhys Lett (EPL)* 1987;4(9):973–7.
- [53] Marwan N, Wessel N, Meyerfeldt U, Schirdewan A, Kurths J. Recurrence-plot-based measures of complexity and their application to heart-rate-variability data. *Phys Rev E* 2002;66:026702.
- [54] Marwan N, Kurths J. Nonlinear analysis of bivariate data with cross recurrence plots. *Phys Lett A* 2002;302(5):299–307.
- [55] Marwan N, Carmen Romano M, Thiel M, Kurths J. Recurrence plots for the analysis of complex systems. *Phys Rep* 2007;438(5):237–329.
- [56] Marwan N. A historical review of recurrence plots. *Eur Phys J Spec Top* 2008;164(1):3–12.
- [57] Goswami B. A brief introduction to nonlinear time series analysis and recurrence plots. *Vibration* 2019;2(4):332–68.
- [58] Vasconcelos DB, Lopes SR, Viana RL, Kurths J. Spatial recurrence plots. *Phys Rev E* 2006;73:056207.
- [59] Matsumoto T. A chaotic attractor from Chua's circuit. *IEEE Trans Circuits Syst* 1984;31:1055–8.
- [60] Belykh VN, Osipov GV, Petrov VS, Suykens JAK, Vandewalle J. Cluster synchronization in oscillatory networks. *Chaos* 2008;18(3):037106.
- [61] Lu W, Liu B, Chen T. Cluster synchronization in networks of coupled nonidentical dynamical systems. *Chaos* 2010;20(1):013120.
- [62] Röhr V, Berner R, Lamei EL, Popovych OV, Yanchuk S. Frequency cluster formation and slow oscillations in neural populations with plasticity. *PLOS ONE* 2019;14(11):1–21.
- [63] dos Santos V, Borges FS, Iarosz KC, Caldas IL, Szezech JD, Viana RL, Baptista MS, Batista AM. Basin of attraction for chimera states in a network of Rössler oscillators. *Chaos* 2020;30(8):083115.
- [64] Menck PJ, Heitzig J, Marwan N, Kurths J. How basin stability complements the linear-stability paradigm. *Nat Phys* 2013;9(2):89–92.
- [65] Rakshit S, Bera BK, Perc M, Ghosh D. Basin stability for chimera states. *Sci Rep* 2017;7(1):1–12.
- [66] Menck PJ, Heitzig J, Marwan N, Kurths J. How basin stability complements the linear-stability paradigm. *Nat Phys* 2013;9(2):89–92.
- [67] Menck PJ, Heitzig J, Kurths J, Joachim Schellnhuber H. How dead ends undermine power grid stability. *Nature Commun* 2014;5(1):3969.

- [68] Schultz P, Heitzig J, Kurths J. Detours around basin stability in power networks. *New J Phys* 2014;16:125001.
- [69] Ott E, Sommerer JC. Blowout bifurcations: the occurrence of riddled basins and on-off intermittency. *Phys Lett A* 1994;188(1):39–47.
- [70] Yanchuk S, Maistrenko Y, Mosekilde E. Synchronization of time-continuous chaotic oscillators. *Chaos* 2003;13(1):388–400.
- [71] Grebogi C, McDonald SW, Ott E, Yorke JA. Final state sensitivity: An obstruction to predictability. *Phys Lett A* 1983;99(9):415–8.
- [72] McDonald SW, Grebogi C, Ott E, Yorke JA. Fractal basin boundaries. *Physica D* 1985;17(2):125–53.
- [73] Grebogi C, Ott E, Yorke JA. Chaos, strange attractors, and fractal basin boundaries in nonlinear dynamics. *Science* 1987;238(4827):632–8.
- [74] Aguirre J, Viana RL, Sanjuán MAF. Fractal structures in nonlinear dynamics. *Rev Modern Phys* 2009;81:333–86.
- [75] Kundu S, Ghosh D. Higher-order interactions promote chimera states. *Phys Rev E* 2022;105:L042202.
- [76] Li X, Ghosh D, Lei Y. Chimera states in coupled pendulum with higher-order interaction. *Chaos Solitons Fractals* 2023;170:113325.